

## EFFECTS OF POROSITY AND HEAT GENERATION ON FREE CONVECTION IN A POROUS TRAPEZOIDAL CAVITY

by

**Mohamed M. MOUSA**

<sup>a</sup>Department of Mathematics, College of Sciences and Human Studies at HowtatSudair,  
Majmaah University, Majmaah, Saudi Arabia

<sup>b</sup>Department of Basic Science, Faculty of Engineering at Benha, Benha University, Benha, Egypt

Original scientific paper  
<https://doi.org/10.2298/TSCI170324245M>

*The problem of laminar free convection in a trapezoidal enclosure, filled with a fluid-saturated porous medium and with internal heat generation has been investigated using a penalty finite element analysis. The enclosure bottom wall is heated at a constant temperature and the top wall is subjected to a constant cold temperature whereas the left inclined wall is considered to be non-isothermal and the right inclined wall is isothermally cooled. The effects of the porosity of the medium and heat generation on the isotherms and streamlines are investigated. The rate of heat transfer from the walls of the cavity is examined as well. The Prandtl number of the fluid is chosen to be 0.7 (air) whereas the value of the Rayleigh number is selected to be  $10^5$ .*

Key words: *finite element method, free convection, fluid-saturated porous medium, heat generation, trapezoidal cavity*

### Introduction

The phenomenon of free convection in cavities of various geometries has received considerable attention in recent years. This is due to its many significant applications in engineering and science such as boilers, systems of nuclear reactor, energy storage and conservation, fire control, chemical, heating, preservation of canned foods and double-panel windows. The investigation of free convection in a trapezoidal enclosure is very challenging compared with classical rectangular or square enclosures due to the existence of inclined walls. The complex geometry of the trapezoidal cavity requires an precise and large effect in code construction and grid generation. In the past few decades, many studies were presented on free convection in trapezoidal enclosures.

Lam *et al.* [1], presented experimental and numerical studies of free convection in trapezoidal enclosures constructed of two vertical isolated side walls, a horizontal hot bottom wall and an inclined cold top wall. Arici and Sahin [2] numerically investigated the natural convection in a partially divided trapezoidal enclosure by using the control volume method. The investigation is done for two different placements of a divider to gether with a non-divider enclosure. The steady free convection of air-flow in a 2-D side-heated trapezoidal room has been numerically investigated by Lasfer *et al* [3]. The geometry considered was, a vertical right cooled sidewall, an inclined left heated sidewall, and two isolated horizontal lower and upper walls. The obtained results showed a great dependence of the heat transfer on inclination angle, the flow fields, Rayleigh number and aspect ratio. Recently, Selimefendigil *et al.* [4] numerically studied

the mixed convection in a lid-driven 3-D flexible walled trapezoidal enclosure with nanofluids using finite element method based on Galerkin weighted residuals. They concluded that the fluid-flow and heat transfer characteristics are influenced by the variations in the elastic modulus of the side wall, Richardson number and volume fraction of nanoparticle for different side wall inclination angles of the trapezoidal cavity.

Extensive investigations have also been carried out to study the heat transfer convection in the fluid-saturated porous medium because of its applicability in various industrial applications concerning the geothermal fields [5], process of phase change [6], applications of heat exchanger [7], bioengineering [8], *etc.* Recently, various studies on free and mixed convection in the porous cavities with many geometrical shapes were carried out by many researchers [9-16]. The trapezoidal enclosures are useful in many applications and many studies were presented in the literature based on the practical applications. Free convective in the trapezoidal cavities (both fluid and porous media) are highly useful for applications in desalination [17], the greenhouse-type solar stills [18], solar cavity receiver [19], *etc.* Although various attempts were made to study the natural convection in irregular porous cavities, the study of effects of heat generation and porosity on natural convection in the porous trapezoidal cavities with linearly heated inclined wall (s) is yet to appear in the literature.

The aim of the current study is to investigate the effects of the porosity of the medium and heat generation on the natural convection in a trapezoidal porous cavity by using the well-known Boussinesq approximation model [20]. The momentum equation including Navier-Stokes inertia term, Brinkman viscous diffusion term and Boussinesq buoyancy term defined with temperatures derived for the porous media in the presence of the of temperature-dependent heat generation effect makes this work discernible. Contextually the present work will focus on the influences of medium porosity and heat generation on the free convection in a trapezoidal cavity filled with fluid saturated porous medium. The obtained numerical results is validated by comparing them with those obtained from a commercial COMSOL Multiphysics software.

### Mathematical formulation

Consider a trapezoidal cavity of height,  $H$ , filled with a fluid-saturated porous medium containing a Newtonian fluid with Prandtl number  $Pr = 0.7$  and initial temperature,  $T_c$ , at rest as shown in fig. 1. The considered porous medium is a non-deformable and homogeneous one, *i.e.* its porosity is constant. The bottom wall of the cavity is uniformly heated at  $T_h$  while the top wall and the top major section of the right inclined wall are maintained at a constant cold temperature  $T_c$ . The temperature condition of the left inclined wall is considered as a non-isothermal type where the temperature reduces linearly from  $T_h$  at the bottom to  $T_c$  at the top. The boundary condition at the lower section of right inclined wall deserves some explanation. This model is based a reactor with a small gap at the bottom of the right inclined wall of length  $s_1 = H/5$  where  $s$  is the right inclined wall side length. This gap is filled with a sodium deposit and the temperature within the gap will vary linearly from  $T_h$  to  $T_c$ . The influence of temperature-dependent heat generation in the flow is also taken into consideration. The heat generation volumetric rate,  $Q$ , is assumed to be:

$$Q = \begin{cases} Q_0 (T - T_c), & T \geq T_c \\ 0, & T < T_c \end{cases} \quad (1)$$

where  $Q_0$  is the heat generation constant. As described in [20], the previous relation is valid for the approximation of the state of some exothermic process and having  $T_c$  as the onset temperature, which means that the heat flows from the surface to the cavity.

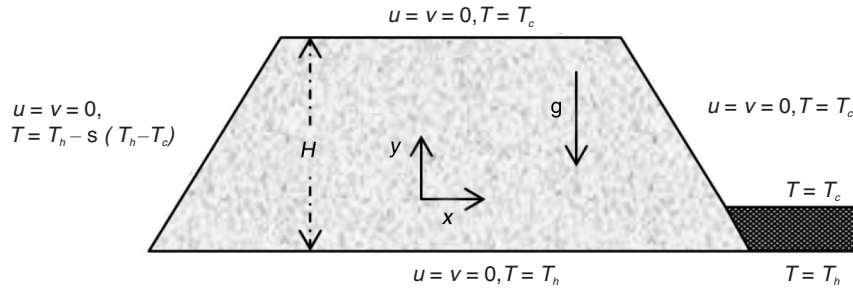


Figure 1. Schematic diagram of the physical and co-ordinate systems

In this study, we assume a steady laminar flow of a viscous incompressible fluid having fixed properties. The well-known Boussinesq approximation is used to include buoyancy effect. Under the previous assumptions, the governing equations for momentum, mass, and energy in a 2-D Cartesian co-ordinate system can be written as:

$$\frac{\partial u}{\partial x} + \frac{\partial v}{\partial y} = 0 \quad (2)$$

$$u \frac{\partial u}{\partial x} + v \frac{\partial u}{\partial y} = -\frac{1}{\rho} \frac{\partial p}{\partial x} + \nu \left( \frac{\partial^2 u}{\partial x^2} + \frac{\partial^2 u}{\partial y^2} \right) - \frac{\nu}{K} u \quad (3)$$

$$u \frac{\partial u}{\partial x} + v \frac{\partial u}{\partial y} = -\frac{1}{\rho} \frac{\partial p}{\partial y} + \nu \left( \frac{\partial^2 v}{\partial x^2} + \frac{\partial^2 v}{\partial y^2} \right) - \frac{\nu}{K} v + g\beta (T - T_c) \quad (4)$$

$$u \frac{\partial T}{\partial x} + v \frac{\partial T}{\partial y} = \alpha \left( \frac{\partial^2 T}{\partial x^2} + \frac{\partial^2 T}{\partial y^2} \right) + \frac{Q_0}{\rho C_p} (T - T_c) \quad (5)$$

where  $u$  and  $v$  are the fluid velocity components in the  $x$ - and  $y$ -directions, respectively  $T$  – the temperature,  $p$  – the pressure,  $K$  – the porous medium permeability,  $\beta$  – the coefficient of volumetric thermal expansion,  $g$  – the gravitational acceleration and  $\rho$ ,  $\nu$ ,  $C_p$  and  $\alpha$  are, respectively, the fluid density, the kinematic viscosity, the specific heat at constant pressure and the thermal diffusivity. The inertia effects of the porous medium have been neglected in the momentum equations, and the viscous dissipation effects are neglected from the energy equation as well. The permeability of the porous medium,  $K$ , is defined by [20],

$$K = \frac{\varepsilon^{+3}}{180 (1 - \varepsilon^+)^2} d^2, \quad (6)$$

where  $\varepsilon^+$  is the media porosity and  $d$  is the solid sphere diameter.

The following dimensionless variables are used in order to non-dimensionalize eqs. (2)-(5):

$$X = \frac{x}{H}, Y = \frac{y}{H}, U = \frac{H}{\nu} u, V = \frac{H}{\nu} v, \theta = \frac{T - T_c}{T_h - T_c}, P = \frac{H}{\rho \nu} p \quad (7)$$

Substituting the dimensionless variables in eqs. (2)-(5), one can obtain the following dimensionless form of the governing equations:

$$\frac{\partial U}{\partial X} + \frac{\partial V}{\partial Y} = 0 \quad (8)$$

$$U \frac{\partial U}{\partial X} + V \frac{\partial U}{\partial Y} = -\frac{\partial P}{\partial X} + \text{Pr} \left( \frac{\partial^2 U}{\partial X^2} + \frac{\partial^2 U}{\partial Y^2} - \gamma U \right) \quad (9)$$

$$U \frac{\partial V}{\partial X} + V \frac{\partial V}{\partial Y} = -\frac{\partial P}{\partial Y} + \text{Pr} \left( \frac{\partial^2 V}{\partial X^2} + \frac{\partial^2 V}{\partial Y^2} - \gamma V \right) + \text{RaPr}\theta \quad (10)$$

$$U \frac{\partial \theta}{\partial X} + V \frac{\partial \theta}{\partial Y} = \frac{\partial^2 \theta}{\partial X^2} + \frac{\partial^2 \theta}{\partial Y^2} + \lambda \theta \quad (11)$$

where

$$\text{Ra} = \frac{g\beta(T_h - T_c)H^3}{\alpha\nu}, \text{Pr} = \frac{\nu}{\alpha}, \gamma = \frac{1}{\text{Da}} = \frac{H^2}{K}, \lambda = \frac{Q_0 H^2}{\rho\nu C_p} \quad (12)$$

where  $\text{Ra}$  is the Rayleigh number,  $\lambda$  – the heat generation parameter, and  $\gamma$  – the porosity parameter which inversely proportional to Darcy number. The corresponding boundary conditions in a dimensionless form will become as follows:

- all boundaries are rigid and non-slip, *i. e.*  $U = V = 0$
- at bottom wall:  $\theta = 1$
- at top wall:  $\theta = 0$
- at left inclined wall:  $\theta = 1 - s$
- at lower part of the right inclined wall:  $\theta = 1 - s/s_1$ , and
- at upper part of the right inclined wall:  $\theta = 0$ .

The heat transfer rate through the cavity walls was quantified using a local and averaged Nusselt number along bottom and top walls of the cavity. Nusselt number represents the ratio of convective to conductive heat transfer across the boundaries. Due to the problem dimensionless representation, the local Nusselt number along the bottom surface, along the top surface and averaged Nusselt number can be defined, respectively:

$$\text{Nu}_0 = -\frac{\partial \theta}{\partial Y} \Big|_{Y=0}, \text{Nu}_H = -\frac{\partial \theta}{\partial Y} \Big|_{Y=H}, \text{Nu}_m = \frac{1}{H} \int_0^H \text{Nu} \, dX \quad (13)$$

The fluid motion is presented by the stream function,  $\psi$ , that will be obtained from velocity components  $U$  and  $V$ :

$$U = \frac{\partial \psi}{\partial Y}, \text{ and } V = -\frac{\partial \psi}{\partial X} \quad (14)$$

Using eq. (14), the following equation can be written:

$$\frac{\partial^2 \psi}{\partial X^2} + \frac{\partial^2 \psi}{\partial Y^2} = \frac{\partial U}{\partial Y} - \frac{\partial V}{\partial X} \quad (15)$$

The boundary condition of the stream function is considered as  $\psi = 0$ , due to the no-slip condition at all boundaries of the cavity.

### Numerical procedure and code validation

The finite element method based on the Galerkin weighted residuals has been used to solve the governing eqs. (8)-(11) subject to the given boundary conditions. The considered technique is well described in [9, 12, 21-24]. Based on the considered method, the cavity domain is discretized into a number of suitable finite elements as a grid. Here, the given domain is composed into non-uniform biquadratic elements. As described in [9, 12, 21-24], the continuity eq. (8) will be used as a constraint and hence the pressure distribution will be obtained using this constraint. To solve eqs. (9)-(11), a penalty finite element method will be used. So, the pressure  $P$  can be removed from eqs. (9) and (10) using the introduced constraint equation:

$$P = -\delta \left( \frac{\partial U}{\partial X} + \frac{\partial V}{\partial Y} \right) \quad (16)$$

where  $\delta$  is a penalty parameter. For large values of  $\delta$ , the continuity equation is satisfied. The typical value of  $\delta$  that provide a consistent solution is  $\delta = 10^7$ . The components of the velocity ( $U$ ,  $V$ ) and temperature ( $T$ ) are expanded using the basis set  $\{\varphi_k\}_{k=1}^N$  as:

$$U \approx \sum_{k=1}^N \varphi_k(X, Y) u_k, \quad V \approx \sum_{k=1}^N \varphi_k(X, Y) v_k, \quad \theta \approx \sum_{k=1}^N \varphi_k(X, Y) \theta_k, \quad \psi = \sum_{k=1}^N \varphi_k(X, Y) \psi_k \quad (17)$$

where  $N$  is the number of nodes of each biquadratic element and  $\varphi_k$  represents the elements shape functions. According to the Galerkin weighted residual finite element technique, the weight functions are the same as the elements shape functions, and hence the non-linear residual equations  $R_i^j$ ,  $i=1, 2, 3, N$ ,  $j=1, 2, 3, 4$  related to eqs. (9)-(11) and (15), respectively, can be easily deduced at nodes of the internal element domain  $\Omega_e$ .

As illustrated in [9, 12, 21], biquadratic shape functions with three point Gaussian quadrature is used to calculate the integrals in the residual equations,  $R_i^j$ . The residual equations are solved using Newton-Raphson method to estimate the coefficients of the expansions in eq. (17). The boundary conditions will be incorporated into the assembled global system of non-linear equations to make it determinate. We use  $L_2$  norm for the residual vectors as a stopping criteria of the Newton-Raphson iterative process. When  $L_2$  norm for each of the variables satisfy the next convergence criteria:

$$\sqrt{\sum (R_i^j)^2} \leq 10^{-6}, \quad j = 1, 2, 3, 4 \quad (18)$$

the solution convergence will be guaranteed.

Eight node biquadratic elements have been used with each element. The co-ordinate  $X$ - $Y$  will be mapped into of the natural co-ordinate  $\zeta$ - $\eta$  because of the irregularity of the element shape before evaluating the Gaussian integration. The transformation between  $(X, Y)$  and  $(\zeta, \eta)$  co-ordinates can be defined by:

$$X = \sum_{k=1}^8 \varphi_k(\zeta, \eta) X_k, \quad \text{and} \quad Y = \sum_{k=1}^8 \varphi_k(\zeta, \eta) Y_k \quad (19)$$

where  $(X_k, Y_k)$  are the  $X, Y$  co-ordinates of the  $k$  nodal points and  $\varphi_k(\zeta, \eta)$  is the local basis function in  $\zeta$ - $\eta$  domain. Here, the eight basis functions used are of a serendipity type [25],

$$\varphi_j = \frac{1}{4} (1 + \zeta\xi)(1 + \eta\eta)(\zeta\xi + \eta\eta - 1) \quad j = 1, 2, 3, 4 \quad (20)$$

$$\varphi_j = \frac{1}{2} (1 + \zeta^2)(1 + \eta\eta) \quad j = 5, 7 \quad (21)$$

$$\varphi_j = \frac{1}{2} (1 + \zeta\xi)(1 - \eta^2) \quad j = 6, 8$$

Thus, the domain integrals in the residual equations are approximated using eight node biquadratic basis functions in  $\zeta$ - $\eta$  domain using eqs. (19) and (20).

Relating to air, the Prandtl number values chosen as 0.7 and the Rayleigh number is considered to be  $10^5$ . Various non-uniform biquadratic grids were constructed over the domain using the commercial grid generator ANSYS. In order to obtain a proper grid distribution with accurate results, a grid independency study is accomplished. The results of the averaged Nusselt number at the bottom hot surfaces for several grid sizes are displayed in tab. 1 for  $\lambda = 0$ ,  $\gamma = 10.0$  and  $\lambda = 10.0$ ,  $\gamma = 0$ . Grid type G4 with 735 number of elements is selected in the subsequent computations.

The results obtained by the present code is validated against the numerical results computed by COMSOL. A comparison between some of the obtained results and those obtained by COMSOL are graphically presented and discussed in the next section. It is worth noting that

the COMSOL results are computed at optimal parameters to guarantee reliability, convergence and accuracy of the solution.

**Table1. Grid independence test of  $Nu_m$  results at the bottom hot surface for  $\lambda = 0, \gamma = 10.0$  and  $\lambda = 10.0, \gamma = 0$**

Grid name	# Elements	$Nu_m$ for $\lambda = 0, \gamma = 10.0$	$Nu_m$ for $\lambda = 10.0, \gamma = 0$
G1	111	0.3634	0.3899
G2	239	0.3991	0.4102
G3	371	0.4016	0.4161
G4	735	0.4084	0.4213

## Results and discussion

Numerical results of free convection heat transfer for a heat-generating fluid in a trapezoidal enclosure filled with a saturated porous medium with uniform porosity subject to a non-uniformly heated left inclined wall are presented in order to determine the effects the medium porosity and heat generation parameter on the isotherms, streamlines and heat transfer inside the enclosure. As declared, the dimensionless controlling parameters are the Rayleigh number, the Prandtl number, the porosity parameter, and the heat generation parameter. Here we have obtained solutions for various values of the porosity and the heat generation parameters.

In figs. 2-5, the contours of the stream function and isotherms are shown for values of  $\lambda$  equal to 0.0, 10.0, 20.0, and 40.0 when  $\gamma$  equal to 0.0, *i. e.* for a pure fluid. figs. 2(a)-5(a), illustrate that the secondary vortex that developed at the left top corner will be grown and divided with the increase of the heat generation parameter,  $\lambda$ . Also, as the heat generation parameter increases, the centre of the primary vortex moves towards the right inclined wall of the cavity. The present investigation is extended for higher values of  $\lambda$  and it has been predicted that two vortices of equal strength would occur at a specific value of  $\lambda$  while with further increase of this parameter, the secondary vortex would be dominant in the cavity.

From fig. 2(b), one can observe that the isotherms are clustered near to the enclosure bottom surface, which means that steep temperature gradients in the upright direction of this area are existed. By comparing figs. 3(b)-5(b) with fig. 2(b), it can be observed that the increase of  $\lambda$  will make the clustered isotherms region moves to right and on the way to the enclosure top cold surface. In the middle of the enclosure, the temperature gradient appears to increase as well. It is predicted that extra increase of the heat generation parameter will make the isotherms to be clustered in the region close to the top surface.

Figure 6 shows Nusselt number distributions along the bottom and top surfaces for different values of the heat generation parameter. From fig. 6(a), it can be drawn that the rate of the heat transfer is low at the left part of the bottom surface and increase in the direction of right part in an oscillation manner due to the conduction of sodium deposit placed in the bottom right corner. Moreover we can conclude that as the heat generation parameter increases, the heat transfer rate from the bottom surface will decrease. This is due to the mechanism of heat generation that will rise the fluid temperature close to the bottom surface, resulting in enlarged resistance to the heat transfer in vertical direction. This conclusion is in a favourably agreement with the results obtained in [20] for a rectangular enclosure. The distribution of heat transfer from the top surface is displayed in fig. 6(b). The top left and right corner zones are inactive regions and heat transfer is mainly caused by conduction. It can be seen that there is a peak value of heat transfer that moves towards the left corner, where the left inclined wall meets the top surface, as the heat generation parameter increases. This peak value increases with the increase of the heat

due to heat generation phenomena. From fig. 6, it can be concluded that the present results is favourably in agreement with COMSOL results for all values of  $\lambda$ .

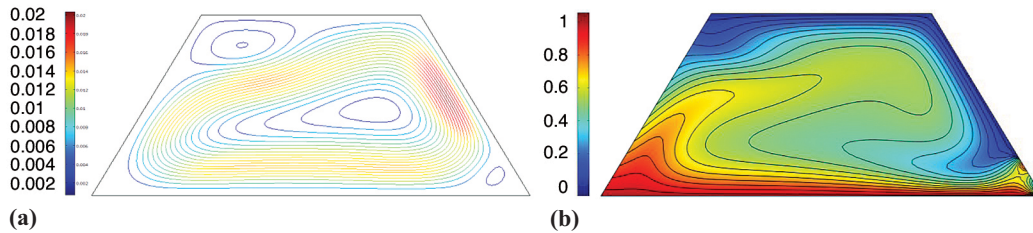


Figure 2. (a) Streamlines and (b) isotherms for  $\lambda = 0.0$  and  $\gamma = 0.0$

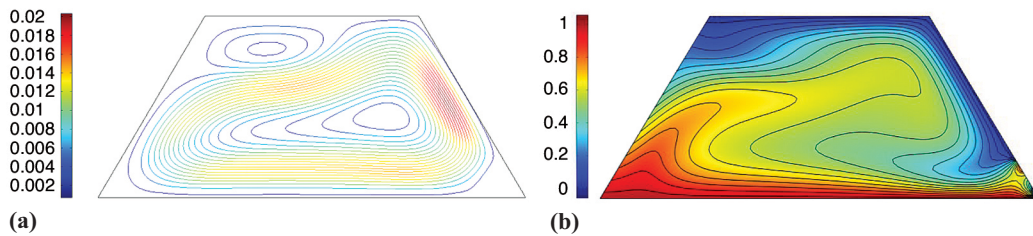


Figure 3. (a) Streamlines and (b) isotherms for  $\lambda = 10.0$  and  $\gamma = 0.0$

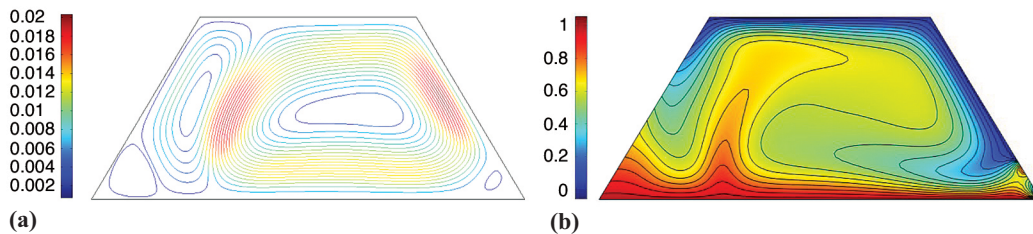


Figure 4. (a) Streamlines and (b) isotherms for  $\lambda = 20.0$  and  $\gamma = 0.0$

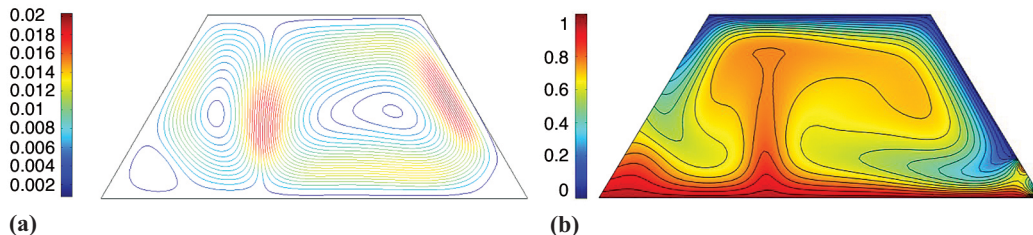


Figure 5. (a) Streamlines and (b) isotherms for  $\lambda = 40.0$  and  $\gamma = 0.0$

The effect of the medium porosity on the isotherms is discussed in fig. 7. The figure presents results for values of the porosity parameter  $\gamma = 10.0, 20.0,$  and  $30.0$  in absence of the heat generation. As shown in fig 7, the temperature gradient decreases as  $\gamma$  increases, as the resistance to fluid flow increases. Also, the effect of flow convection decreases as the porosity parameter increases. It is expected that extra increase of the porosity parameter, which is accompanied by a decrease in Darcy number, will make the temperature distributions and clustered isotherms more uniformly.

In fig. 8, the effects of the medium porosity on the heat transfer from the bottom and top surfaces are discussed in absence of heat generation. In this figure, the heat transfer distribution is displayed for values of the porosity parameter  $\gamma = 0.0, 10.0, 20.0,$  and  $30.0$  fig. 8(a) illustrates that,

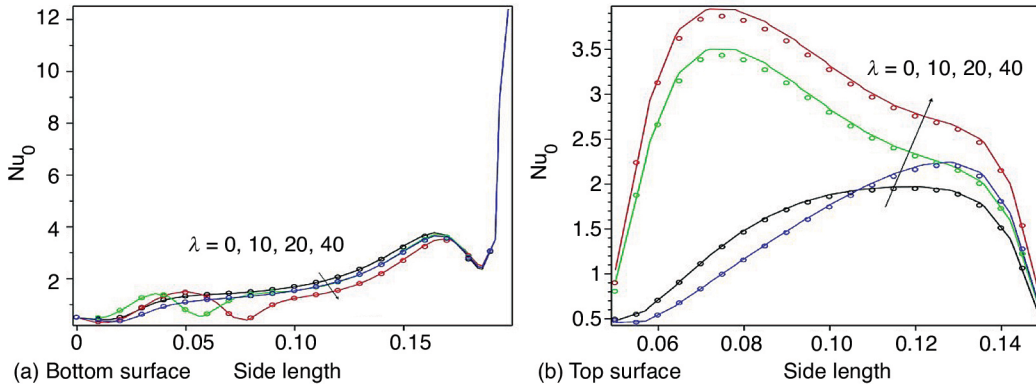


Figure 6. Local Nusselt number distribution along the bottom and top surface for different values of  $\lambda$  when  $\gamma = 0.0$  using present code results (solid lines) and COMSOL results (open circles)

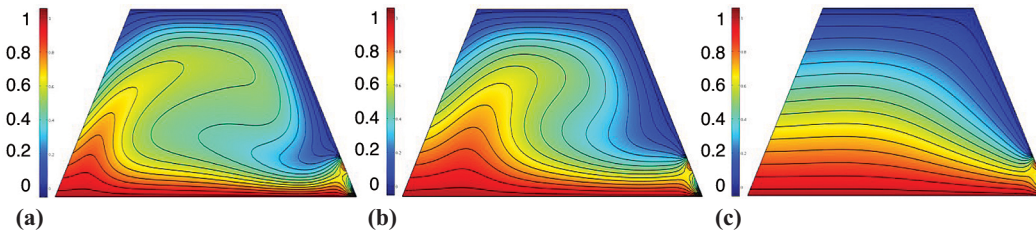


Figure 7. Isotherms for (a)  $\gamma = 10.0$ , (b)  $\gamma = 20.0$ , and (c)  $\gamma = 30.0$  while  $\lambda = 0.0$

the heat transfer from the bottom wall decreases as the porosity parameter increases. From fig. 8(b), it can be seen that there is a peak value of heat transfer that decreases with the increasing of  $\gamma$ . In general, as the porosity parameter increases, the heat transfer decreases from the bottom and top surfaces. This result was mentioned in [20] in case a rectangular enclosure. The previous result can be rewritten as, the heat transfer from the bottom and top surfaces enhances with increasing values of Darcy number. It is worth noting that figs. 6 and 8 demonstrate a good agreement between the results obtained with the present code and those obtained with the COMSOL model for all values of  $\lambda$  and  $\gamma$ . This agreement can be considered as a sufficient validation of the present study.

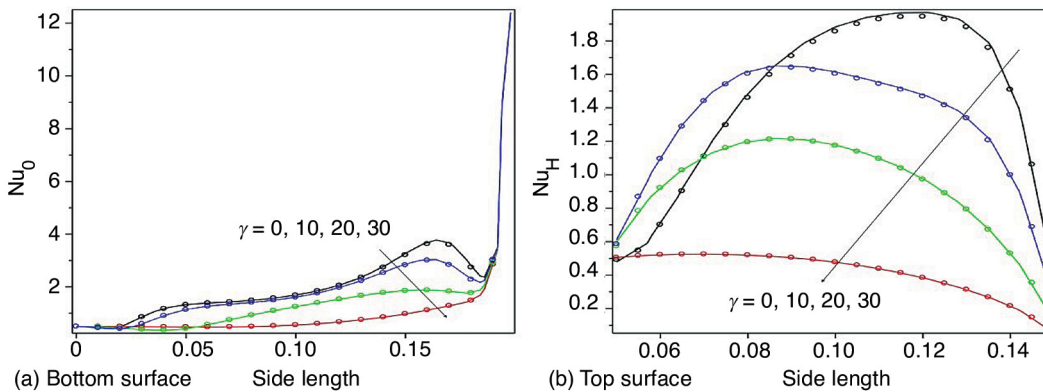


Figure 8. Local Nusselt number distribution along the bottom and top surfaces for different values of  $\gamma$  when  $\lambda = 0.0$  using present code results (solid lines) and COMSOL results (open circles)

Figure 9 shows the averaged Nusselt number along the bottom and top surfaces for various heat generation parameter when  $\gamma = 0.0$  and medium porosity parameter when  $\lambda = 0.0$ . As shown in fig. 9(a), the averaged heat transfer enhances as the value of the porosity parameter decreases, *i. e.* as the Darcy number increases, due to the increasing in the porous medium permeability. Figure 9(b) illustrates that the averaged heat transfer from the top surface increases while from the bottom surface decreases as the heat generation parameter enhances.

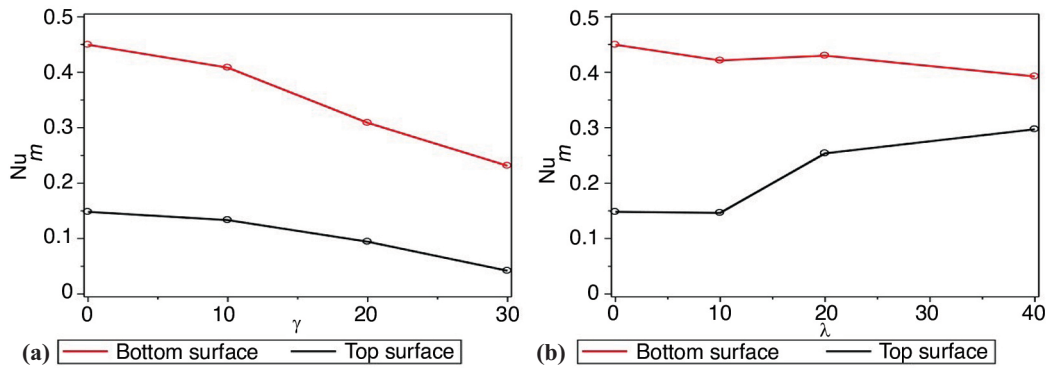


Figure 9. Averaged Nusselt number along the bottom and top surfaces vs. (a)  $\gamma$  when  $\lambda = 0.0$  and (b)  $\lambda$  when  $\gamma = 0.0$

### Conclusion

In this study, the effects of medium porosity and heat generation on the free convection of a laminar flow and heat transfer in a non-isothermal trapezoidal enclosure have been investigated using a finite element method. The problem of buoyancy effects is treated using Boussinesq approximation. From the presented results, It can be concluded that the increasing of heat generation in the fluid will reduce thermal gradients near the heated bottom wall of the enclosure and leads to increase thermal gradients at the cold top wall. The main vortex strength induced by buoyancy is decreased due to the increasing of heat generation, and additional closely like double vortex structure grows. In absence of the heat generation, the averaged heat transfer from the enclosure surfaces enhances as the values of Darcy number increases and porosity parameter decreases, due to the increasing in the permeability of the porous medium. Finally, the reliability of the present results was confirmed by comparing them with the results obtained by COMSOL model.

### Acknowledgment

The author would like to thank the Deanship of Scientific Research of Majmaah University for providing financial support under the research grant No. 26/37, 1437/1438 H.

### Nomenclature

$C_p$	– specific heat, [ $\text{Jkg}^{-1}\text{K}^{-1}$ ]	$Q$	– heat generation volumetric rate, [ $\text{Wm}^{-3}$ ]
$Da$	– darcy number, ( $= K/H^2$ ), [–]	$s$	– right inclined wall side length [m]
$g$	– gravitational acceleration, [ $\text{ms}^{-2}$ ]	$T$	– absolute temperature, [K]
$H$	– trapezoidal cavity height [m]	$T_c$	– initial temperature, [K]
$K$	– permeability of the porous media, [ $\text{m}^2$ ]	$T_h$	– high temperature, [K]
$Ra$	– rayleigh number $\{= [g\beta(T_h - T_c)H^3]/\alpha\nu\}$ , [–]	$U$	– dimensionless horizontal velocity, [–]
$Nu_0$	– bottom wall Nusselt number, [–]	$u$	– horizontal velocity, [ $\text{ms}^{-1}$ ]
$Nu_H$	– top wall Nusselt number, [–]	$V$	– vertical velocity, [ $\text{ms}^{-1}$ ]

$Nu_m$	– averaged Nusselt number, [–]	$v$	– dimensionless vertical velocity, [–]
$P$	– dimensionless fluid pressure, [–]	$X, Y$	– dimensionless co-ordinates, [–]
$Pr$	– prandtl number, ( $= \nu/\alpha$ ), [–]	$x, y$	– cartesian co-ordinates, [m]
$p$	– fluid pressure, [ $Nm^{-2}$ ]	<i>Greek symbols</i>	
$Q$	– heat generation volumetric rate, [ $Wm^{-3}$ ]	$\alpha$	– thermal diffusivity, [ $m^2s^{-1}$ ]
$s$	– right inclined wall side length [m]	$\beta$	– thermal expansion coefficient, [ $K^{-1}$ ]
$T$	– absolute temperature, [K]	$\gamma$	– porosity parameter, ( $=1/Da$ ), [–]
$T_c$	– initial temperature, [K]	$\delta$	– penalty parameter, [–]
$T_h$	– high temperature, [K]	$\theta$	– dimensionless temperature, [–]
$U$	– dimensionless horizontal velocity, [–]	$\nu$	– kinematic viscosity, [ $m^2s^{-1}$ ]
$u$	– horizontal velocity, [ $ms^{-1}$ ]	$\lambda$	– heat generation parameter, [–]
$V$	– vertical velocity, [ $ms^{-1}$ ]	$\zeta, \eta$	– natural co-ordinate, [–]
$v$	– dimensionless vertical velocity, [–]	$\rho$	– fluid density at temperature $T_c$ , [ $kgm^{-3}$ ]
$X, Y$	– dimensionless co-ordinates, [–]	$\psi$	– dimensionless stream function, [–]
$x, y$	– cartesian co-ordinates, [m]		

## References

- [1] Lam, S., *et al.*, Experimental and Numerical Studies of Natural Convection in Trapezoidal Cavities, *ASME J. Heat Transfer*, 111 (1989), 2, pp. 372-377
- [2] Arici, M. E., Sahin, B., Natural Convection Heat Transfer in a Partially Divided Trapezoidal Enclosure, *Thermal Science*, 13 (2009), 4, pp. 213-220
- [3] Lasfer, K., *et al.*, Numerical Study of Laminar Natural Convection in a Side-Heated Trapezoidal Cavity at Various Inclined Heated Sidewalls, *Heat Transfer Eng.*, 31 (2010), 5, pp. 362-373
- [4] Selimefendigil, F., *et al.*, Analysis of Mixed Convection of Nanofluid in a 3D Lid-Driven Trapezoidal Cavity with Flexible Side Surfaces and Inner Cylinder, *International Communications in Heat and Mass Transfer*, 87 (2017), Oct., pp. 40-51
- [5] Weir, G. J., The Relative Importance of Convective and Conductive Effects in Two-Phase Geothermal Fields, *Transport Porous Media*, 16 (1994), 3, pp. 289-298
- [6] Gao, D., Chen, Z., Lattice Boltzmann Simulation of Natural Convection Dominated Melting in a Rectangular Cavity Filled with Porous Media, *Int. J. Therm. Sci.*, 50 (2011), 4, pp. 493-501
- [7] Abdesslem, J., *et al.*, Radiative Properties Effects on Unsteady Natural Convection Inside a Saturated Porous Medium: Application for Porous Heat Exchangers, *Energy*, 61 (2013), Nov., pp. 224-233
- [8] Khaled, A. R. A., Vafai, K., The Role of Porous Media in Modeling Flow and Heat Transfer in Biological Tissues, *Int. J. Heat Mass Transfer*, 46 (2003), 26, pp. 4989-5003
- [9] Mousa, M. M., Finite Element Investigation of Stationary Natural Convection of Light and Heavy Water in a Vessel Containing Heated Rods, *Zeitschrift für Naturforschung A*, 67a (2012), 6/7, pp. 421-427
- [10] Darvishi, M. T., *et al.*, Natural Convection Heat Transfer in a Partially Divided Trapezoidal Enclosure, *Thermal Science*, 19 (2015), 2, pp. 669-678
- [11] Rahman, M. M., *et al.*, Unsteady Mixed Convection in a Porous Media Filled Lid-Driven Cavity Heated by a Semi-Circular Heaters, *Thermal Science*, 19 (2015), 5, pp. 1761-1768
- [12] Mousa, M. M., Modeling of Laminar Buoyancy Convection in a Square Cavity Containing an Obstacle, *Bulletin of the Malaysian Mathematical Sciences Society*, 39 (2016), 2, pp. 483-498
- [13] Selimefendigil, F., Modeling and Prediction of Effects of Time-Periodic Heating Zone on Mixed Convection in a Lid-Driven Cavity Filled with Fluid-Saturated Porous Media, *Arab. J. Sci. i Eng.*, 41 (2016), 11, pp. 4701-4718
- [14] Selimefendigil, F., *et al.*, Mixed Convection in Superposed Nanofluid and Porous Layers in Square Enclosure with Inner Rotating Cylinder, *International Journal of Mechanical Sciences*, 124-125 (2017), May, pp. 95-108
- [15] Ismael, M. A., *et al.*, Mixed Convection in a Vertically Layered Fluid-Porous Medium Enclosure with Two Inner Rotating Cylinders, *Journal of Porous Media*, 20 (2017), 6, pp. 491-511
- [16] Sheremet, M.A., Pop, I., Free Convection in Wavy Porous Enclosures with Non-Uniform Temperature Boundary Conditions Filled with a Nanofluid: Buongiorno's Mathematical Model, *Thermal Science*, 21 (2017), 3, pp. 1183-1193

- [17] Aramayo, A. M., *et al.*, Conjugate Heat Transfer in a Two Stage Trapezoidal Cavity Stack, *Lat.Am. Appl. Res.*, 39 (2009), 1, pp. 1-9
- [18] Papanicolaou, E., Belessiotis, V., Double-Diffusive Natural Convection in an Asymmetric Trapezoidal Enclosure: Unsteady Behavior in the Laminar and the Turbulent-Flow Regime, *Int. J. Heat Mass Transfer*, 48 (2005), 1, pp. 191-209
- [19] Reddy, K. S., Kumar, K. R., Estimation of Convective and Radiative Heat Losses from an Inverted Trapezoidal Cavity Receiver of Solar Linear Fresnel Reflector System, *Int. J. Therm. Sci.*, 80 (2014), June, pp. 48-57
- [20] Hossain, M. A., Wilson, M., Natural Convection Flow in a Fluid-Saturated Porous Medium Enclosed by Non Isothermal Walls with Heat Generation, *Int. J. Therm. Sci.*, 41 (2002), 5, pp. 447-454
- [21] Mousa, M. M., Finite Element Simulation of a Unimolecular Thermal Decomposition Inside a Reactor, *Journal of Applied Mathematics and Physics*, 4 (2016), 2, pp. 328-340
- [22] Basak, T., Ayappa, K. G., Influence of Internal Convection During Microwave Thawing of Cylinders, *AIChE J.*, 47 (2001), 4, pp. 835-850
- [23] Nassehi, V., Parvazinia, M., *Finite Element Method in Engineering*, Imperial College Press, London, 2010
- [24] Parvin, S., Nasrin, R., Analysis of the flow and heat transfer characteristics for MHD free convection in an enclosure with a heated obstacle, *Non-linear Analysis: Modelling and Control* 16 (2011), 1, pp. 89-99
- [25] Liu, G. R., Quek, S. S., *The Finite Element Method: A Practical Course*, Butterworth-Heinemann, New York, USA, 2003